INSTITUTE OF PHYSICS PUBLISHING JOURNAL OF PHYSICS D: APPLIED PHYSICS

J. Phys. D: Appl. Phys. **38** (2005) 2543–2555 doi:10.1088/0022-3727/38/15/004

Optical properties of human skin, subcutaneous and mucous tissues in the wavelength range from 400 to 2000 nm

A N Bashkatov[1], **E A Genina, V I Kochubey and V V Tuchin**

Institute of Optics and Biophotonics, Saratov State University, 83, Astrakhanskaya Str., Saratov, 410012, Russia

E-mail: bash@optics.sgu.ru

Received 11 January 2005, in final form 7 April 2005
Published 22 July 2005
Online at stacks.iop.org/JPhysD/38/2543

Abstract

The optical properties of human skin, subcutaneous adipose tissue and human mucosa were measured in the wavelength range 400–2000 nm. The measurements were carried out using a commercially available spectrophotometer with an integrating sphere. The inverse adding–doubling method was used to determine the absorption and reduced scattering coefficients from the measurements.

1. Introduction

The development of optical methods in modern medicine in the areas of diagnostics, therapy and surgery has stimulated the investigation of optical properties of various biological tissues, since the efficacy of laser treatment depends on the photon propagation and fluence rate distribution within irradiated tissues. Examples of diagnostic use are the monitoring of blood oxygenation and tissue metabolism [1, 2], laser Doppler flowmetry [3], pulse oximetry [4], detection of cancer by fluorescence [5, 6] and spectrophotometric methods [7, 8] and various techniques recently suggested for optical imaging [9–11]. Therapeutic uses include applications in laser surgery [12], laser angioplasty and ablation [13–16] and in photodynamic therapy [17–25]. For these applications, knowledge of tissue optical properties is of great importance for interpretation and quantification of diagnostic data, and for prediction of light distribution and absorbed dose for therapeutic use. The knowledge of tissue optical properties is also necessary for the development of novel optical technologies of photodynamic and photothermal therapy, optical tomography, optical biopsy, etc. Numerous investigations related to determination of tissue optical properties are available. However, the optical properties of many tissues have not been studied in a wide wavelength range.

Review of the literature [5, 6, 17, 19, 21–36] shows that skin and mucous are the most important tissues for photodynamic therapy of cancer and other diseases. Many authors have studied optical properties of these tissues. Recently the skin optical properties have been measured with the integrating sphere technique in the visible and near-infrared (NIR) spectral ranges by Prahl [37], Chan *et al* [38], Simpson *et al* [39], Du *et al* [40] and Troy and Thennadil [41], but the presented data are characteristically different, especially in the IR spectral range. Knowledge of the optical properties of subcutaneous adipose tissue is also important, since optical properties of this tissue layer determine light distribution in the irradiated skin in the course of photodynamic treatment. In addition, analysis of adipose tissue absorption and scattering properties in a wide wavelength range is essential for developing novel optical technologies for treatment of obesity and cellulite, as, evidently, the optical technologies promise less danger to the patient than the widely used surgical and pharmaceutical treatments.

Investigation of the mucous optical properties is necessary for light dosimetry in photodynamic therapy of bladder, colon, oesophagus, stomach, etc. The treatment of purulent maxillary sinusitis is an important problem in modern rhinology, despite the wide application of surgical and pharmaceutical methods [42, 43]. One of the new methods of treatment of this disease is photodynamic therapy of the mucous membrane of the maxillary sinus [42]. The optical properties of mucous tissues were shown by Müller and Roggan [44] for the wavelength 1064 nm. However, in a wide wavelength range the optical properties of mucous tissues have not been studied.

The goal of this paper is to measure the absorption and reduced scattering coefficients of human skin, subcutaneous adipose tissue and mucous in the wavelength range from 400 to 2000 nm.

[1] Author to whom any correspondence should be addressed.

2. Physical properties and structure of the investigated tissues

The skin presents a complex heterogeneous medium, where the blood and pigment content are spatially distributed variably in depth [45–48]. The skin consists of three main visible layers from the surface: epidermis (100 μm thick, the blood-free layer), dermis (1–4 mm thick, vascularized layer) and subcutaneous fat (from 1 to 6 mm thick, in dependence from the body site). Typically, the optical properties of the layers are characterized by the absorption and scattering coefficient, which equals the average number of absorption and scattering events per unit path length of photon travel in the tissue and the anisotropy factor, which represents the average cosine of the scattering angles.

The randomly inhomogeneous distribution of blood and various chromophores and pigments in skin produces variations of the average optical properties of the skin layers. Nonetheless, it is possible to define the regions in the skin, where the gradient of skin cells structure, chromophores or blood amounts, changing with a depth, which roughly equals zero [45]. This allows subdivision of these layers into sublayers, where the physiological nature, physical and optical properties of their cells and pigments content are concerned. The epidermis can be subdivided into two sublayers: non-living and living epidermis. Non-living epidermis or stratum corneum (about 20 μm thick) consists of only dead squamous cells, which are highly keratinized with a high lipid and protein content, and has a relatively low water content [45, 46, 48]. Living epidermis (100 μm thick) contains most of the skin pigmentation, mainly melanin, which is produced in the melanocytes [49]. Large melanin particles such as melanosomes (>300 nm in diameter) exhibit mainly forward scattering. Whereas, melanin dust, whose particles are small (<30 nm in diameter) has the isotropy in the scattering profile and optical properties of the melanin particles (30–300 nm in diameter) may be predicted by the Mie theory.

The dermis is a vascularized layer and the main absorbers in the visible spectral range are the blood haemoglobin, carotene and bilirubin. In the IR spectral range absorption properties of skin dermis are determined by the absorption of water. Following the distribution of blood vessels, [47] skin dermis can be subdivided into four layers: the papillary dermis (150 μm thick), the upper blood net plexus (100 μm thick), the reticular dermis (1–4 mm thick) and the deep blood net plexus (100 μm thick).

The scattering properties of the dermal layers are defined mainly by the fibrous structure of the tissue, where collagen fibrils are packed in collagen bundles and have lamellae structure. The light scatters on both single fibrils and scattering centres, which are formed by the interlacement of the collagen fibrils and bundles. To sum up, the average scattering properties of the skin are defined by the scattering properties of the reticular dermis because of the relatively big thickness of the layer (up to 4 mm [48]) and comparable scattering coefficients of the epidermis and the reticular dermis. Absorption of haemoglobin and water of the skin dermis and lipids of the skin epidermis define absorption properties of the whole skin. It should be noted that absorption of haemoglobin is defined by the haemoglobin oxygen saturation, since absorption coefficients of haemoglobin are different for oxy and deoxy forms. For an adult the arterial oxygen saturation is generally above 95% [4]. Typical venous oxygen saturation is 60–70% [1]. Thus, absorption properties of blood have been defined by absorption of both oxy and deoxy forms of haemoglobin.

The subcutaneous adipose tissue is formed by aggregation of fat cells (adipocytes) containing stored fat (lipids) in the form of a number of small droplets for lean or normal humans and a few or even a single big drop in each cell for obese humans; the lipids are mostly represented by triglycerides [50, 51]. Content of the lipids in a single adipocyte is about 95% of its volume. The diameters of the adipocytes are in the range 15–250 μm [52] and their mean diameter ranges from 50 [50] to 120 μm [51]. In the spaces between the cells there are blood capillaries (arterial and venous plexus), nerves and reticular fibrils connecting each cell and providing metabolic activity to the fat tissue [50, 51]. Absorption of the human adipose tissue is defined by absorption of haemoglobin, lipids and water. The main scatterers of adipose tissue are spherical droplets of lipids, which are uniformly distributed within adipocytes.

The mucous membrane plays a leading role in the physiology of the nose and paranasal sinuses [43, 53]. It is covered with a pseudostratified epithelium, which consists of ciliated, columbar as well as short and long inserted epithelial cells. The membrane called basic divides epithelial and proper layers of the mucous tissue and consists of reticular fibrils, which are located in the interstitial homogeneous media. The membrane does not have a constant thickness. In the case of hyperplasia of the mucous membrane, the membrane thickens considerably [54].

The proper layer of the mucous membrane is similar in structure to connective tissue, consisting of collagen and elastin fibrils. The interstitial fluid of the mucous membrane contains proteins and polysaccharides and is similar in composition to the interstitial fluid of most of the connective tissues. The proper layer of the mucous membrane consists of three sublayers. A subepithelial (or lymphoid) layer contains a great amount of leukocytes. In the intermediate sublayer of the proper layer, tubuloalveolar glands are contained. In the deep sublayer of the proper layer, venous plexuses are arranged, which consist of a surface network of smaller vessels and a deeper network of larger vessels. Normally, the total thickness of the mucous membrane varies from 0.1 to 0.5 mm [43, 53]. In the presence of pathology (maxillary sinusitis, rhinitis or other rhinological disease), the thickness of the mucous membrane increases considerably and can reach 2–3 mm [43]. It should be noted that the proper layer of the mucous membrane is the main layer protecting against micro-organisms causing infectious diseases [53]. The optical properties of the mucous membranes are determined mainly by the optical properties of the proper layer since this layer is much thicker than the epithelial layer.

3. Materials and methods

Measurements have been carried out *in vitro* with skin samples obtained from *post-mortem* examinations and fresh human subcutaneous adipose tissue samples taken from the peritoneum area of patients during planned surgery. Optical

properties of the mucous membrane of the maxillary sinuses were measured for samples, which were obtained from patients with chronic maxillary sinusitis during planned surgery. All tissue samples were kept in saline at room temperature of about 20°C until spectroscopic measurements were carried out. The skin tissue samples were measured one day after autopsy. The adipose tissue samples were measured during 3–4 h after biopsy, and the mucous tissue samples were measured during 2–3 h after biopsy. All the tissue samples were cut into pieces each with an area of about $20 \times 20\,\mathrm{mm}^2$. For mechanical support, the tissue samples were sandwiched between two glass slides. Since compression of tissue causes an increase in the tissue absorption and scattering coefficients [38], in the measurements of the tissue the samples were sandwiched without (or with minimal) compression. In order to provide optical contact between the sample and the glass slides and to prevent the sample compression, the distance between the glass slides was regulated by a special plastic bush, whose thickness varied according to the samples thickness. The thickness of each tissue sample was measured with a micrometer in several points over the sample surface and averaged. Precision of the single measurement was $\pm 50\,\mu$m.

The total transmittance and diffuse reflectance measurements have been performed in the 400–2000 nm wavelength range using the commercially available CARY-2415 ('Varian', Australia) spectrophotometer with an integrating sphere. The inner diameter of the sphere is 100 mm, the size of the entrance port is 20×20 mm and the diameter of the exit port is 16 mm. As a light source, a halogen lamp with filtering of the radiation in the studied spectral range has been used in the measurements. The diameter of incident light beam on the tissue sample is 3 mm. The scan rate is $2\,\mathrm{nm\,s}^{-1}$.

For processing the experimental data and determination of the optical properties of the tissue, the inverse adding–doubling (IAD) method developed by Prahl *et al* [55] has been used. The method is widely used in tissue optics for processing the experimental data of spectrophotometry with integrating spheres [41, 56–60]. This method allows one to determine the absorption (μ_a) and the reduced scattering coefficients ($\mu_s' = \mu_s(1-g)$) of a tissue from the measured values of the total transmittance and the diffuse reflectance. Here μ_s is the scattering coefficient and g is the anisotropy factor of scattering. In these calculations the anisotropy factor has been fixed at 0.9, since this value is typical for many tissues in the visible and NIR spectral ranges [17]. The main advantage of the IAD method, when compared with many other methods of solution of the radiative transfer equation, is related to its validation for the arbitrary ratio of the absorption and scattering coefficients [55]. The property of the IAD method becomes very important in the case of determination of the optical properties of tissues within strong absorption bands, when the values of the absorption and scattering coefficients become comparable. Other methods, such as the diffusion approximation [61–63] or the Kubelka–Munk method [64–66], require, for their applicability, a fulfilment of the condition $\mu_a/\mu_s \ll 1$. The inverse Monte Carlo technique [67] can also be used for the arbitrary ratio of μ_a and μ_s, but requires very extensive calculations. The main limitation of the IAD method is that there may be a possible loss of scattering radiation through the lateral sides of a sample, at calculations [68]. Loss of light through the sides of the sample and the sample holder may erroneously increase the calculated value of the absorption coefficient. These losses depend on the physical size and geometry of the sample, i.e. the losses existing in the case when the sizes of a sample do not significantly exceed the diameter of the incident beam. The size of the exit and the entrance ports of the integrating sphere are also important for errorless measurements of the total transmittance and diffuse reflectance [68]. The tissue sample should completely cover the port in the integrating sphere, and the distance from the edge of the irradiating beam on the sample to the edge of the port should be much larger than the lateral light propagation distance, which is determined by $1/(\mu_a + \mu_s')$. If this is not satisfied, then light will be lost from the sides of the sample and the loss will be attributed to absorption, and so the absorption coefficient will be overestimated. These requirements have been met in our experiments, since maximal size of the sphere port does not exceed 20 mm, whereas the minimal size of the tissue samples is 20 mm. In addition, using the absorption and the reduced scattering coefficients of the investigated tissues presented below, in the next section, we calculated the lateral light propagation distance. For the skin, the maximal lateral light propagation distance is equal to 0.7 mm for the wavelength 1929 nm. For the subcutaneous adipose tissue the maximal value of the lateral light propagation distance is equal to 1.25 mm for the wavelength 1620 nm. For the mucous tissue, the value is equal to 2.2 mm for the wavelength 1284 nm. Taking into account the diameter of the incident beam (3 mm), the minimal size of a tissue sample has to be larger than 7.5 mm, which was satisfied for each tissue sample under study. It is seen that the lateral light propagation distance is smaller than the distance from the edge of the irradiating beam on the sample to the sample port edge. In addition, Pickering *et al* [68] reported that the area of tissue sample has to be smaller than the area of the inner surface of the integrating sphere. This requirement has also been met in our experiments, since the area of the inner surface of integrating sphere used in the measurements was $314.16\,\mathrm{cm}^2$, whereas the area of any tissue sample did not exceed $5.0\,\mathrm{cm}^2$. Figure 1 shows geometry and parameters of the measurements in the transmittance and reflectance modes, respectively.

Calculation of tissue optical properties was performed for each wavelength point. The algorithm consists of the following steps: (a) estimation of a set of optical properties; (b) calculation of the reflectance and transmittance with the adding–doubling iterative method; (c) comparison of the calculated with the measured values of the reflectance and the transmittance; (d) iteration of the above steps until a match (within the specified acceptance margin) is reached. With this iterative process the set of optical properties that yields the closest match to the measured values of reflectance and transmittance are taken as the optical properties of the tissue.

For estimation of the mean size of scatterers of the investigated tissues, the spectroturbidimetric method described in [69] has been used. This method is based on approximation of the scattering coefficient μ_s of turbid media by a power law $\mu_s = a\lambda^{-w}$, where parameter a is defined by the concentration of particles in the media. The wavelength exponent w is independent of the particle concentration and characterizes the

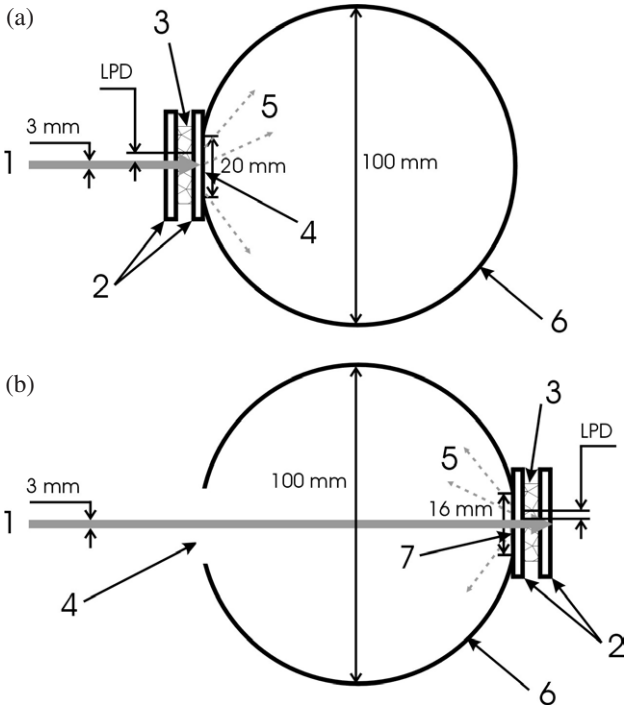

Figure 1. The geometry of the measurements in (*a*) transmittance mode (*b*) reflectance mode. 1—the incident beam (diameter 3 mm); 2—the glass slides; 3—the tissue sample; 4—the entrance port (square 20 × 20 mm); 5—the transmitted (or diffuse reflected) radiation; 6—the integrating sphere (inner diameter is 100 mm); 7—the exit port (diameter 16 mm). LPD—the maximal value of lateral light propagation distance (0.7 mm for skin, 1.25 mm for subcutaneous adipose tissue and 2.2 mm for mucous tissue under study).

mean size of the particles and defines the spectral behaviour of the scattering coefficient [69]. Both the parameter a and the wavelength exponent w are defined by the ratio of refractive indices of the scatterers and environment medium [69]. In experiments, w is expressed in terms of the scattering coefficients measured in a small enough spectral interval (about 200 nm) by the relationship $w = -\partial \ln \mu_s / \partial \ln \lambda$. The substitution in the relationship of a theoretical expression for μ_s obtained for some disperse system models results in equations for determination of either the particle size or the particle refractive index [69]. In the first case, the particle refractive index has to be determined beforehand in independent experiments or has to be obtained from the literature. As a first approximation, w can be calibrated by the formula

$$w(x, m) = \frac{\partial \ln Q(x, m)}{\partial \ln x} \tag{1}$$

with the scattering efficiency factor $Q(x, m)$ calculated for monodisperse system of homogeneous spherical (or cylindrical) isotropic particles. Note that the scattering coefficient μ_s can be connected with the scattering efficiency factor $Q(x, m)$ by the relationship $\mu_s(x, m) = N(\pi d^2/4)Q(x, m)$. Here $m = n_s/n_I$ is the relative refractive index of the scattering particles, i.e. the ratio of the refractive indices of the scatterers (n_s) and the ground materials (i.e. interstitial fluid) (n_I) and x is the dimensionless relative size of scatterers, which is determined as $x = \pi d n_I/\lambda$, where λ is the wavelength, d the diameter of the particles and N the number of scattering particles in the unit of volume.

In the case of spectrophotometric measurements with integrating sphere technique, measured parameter is the reduced scattering coefficient and wavelength dependence of the reduced scattering coefficient can be approximated in accordance with a power law [69–72]

$$\mu_s'(\lambda) = a\lambda^{-w}. \tag{2}$$

On the other hand, the reduced scattering coefficient can be calculated for monodisperse system of spherical particles with the formula $\mu_s'(x, m) = N(\pi d^2/4)Q'(x, m)$, where $Q'(x, m) = Q(x, m)(1 - g)$.

In this case equation (1) can be rewritten in the form

$$w(x, m) = \frac{\partial \ln Q'(x, m)}{\partial \ln x}. \tag{3}$$

In this study, calculation of the scattering efficiency factor $Q(x, m)$ and anisotropy factor g has been performed in accordance with the Mie scattering model, using the algorithm presented by Bohren and Huffman [73].

The mean diameter of the scattering particles has been obtained by minimization of the target function

$$F(x) = (w(x, m) - w^{\exp})^2 \tag{4}$$

with the boundary condition $0.7 \leqslant g \leqslant 0.95$. Here $w(x, m)$ is the wavelength exponent calculated with equation (3) and $w^{\exp}$ is the experimentally measured wavelength exponent value from equation (2). When parameter x was estimated then the mean diameter of the scattering particles was calculated from the relation $d = x\lambda/(\pi n_I)$. In this calculation the refractive indices n_s and n_I for corresponding wavelengths have been obtained from literature.

To minimize the target function, the Levenberg–Marquardt nonlinear least-squares-fitting algorithm, described in detail by Press *et al* [74], has been used. Iteration procedure is repeated until the experimental and the calculated data are matched. As a termination condition of the iteration process, we have used the expression $|w(x, m) - w^{\exp}|/w^{\exp} \leqslant 0.01$.

4. Results and discussion

4.1. Skin optical properties

Twenty-one skin samples obtained from post-mortem examinations were used for the *in vitro* measurements. Figures 2(*a*) and (*b*) and 3(*a*) and (*b*) show the measured optical properties of the human skin samples calculated by the IAD method on the basis of measured values of the total transmittance and the diffuse reflectance. Figure 2(*a*) presents the wavelength dependence of the skin absorption coefficient. The vertical lines correspond to the values of standard deviation (SD), which is determined by SD $= \sqrt{\sum_{i=1}^{N}(\bar{\mu}_a - \mu_{ai})^2/n(n-1)}$, where $n = 21$ is the number of the measured tissue samples, μ_{ai} is the absorption coefficient of each sample and $\bar{\mu}_a$ is the mean value of the absorption coefficient for each wavelength, which is calculated as $\sum_{i=1}^{N} \mu_{ai}/n$. In the visible spectral range of the spectrum,

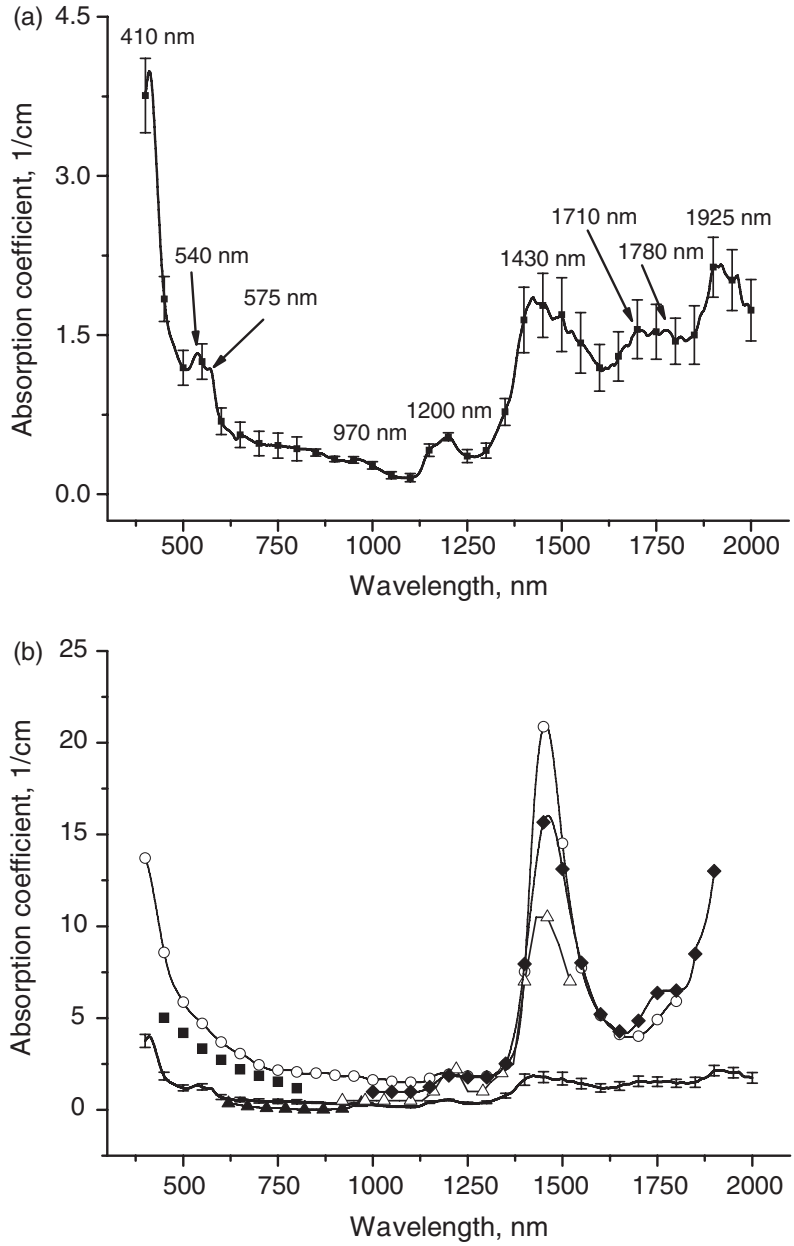

Figure 2. The wavelength dependence of the absorption coefficient μ_a of human skin *in vitro*. (*a*) The vertical lines show the SD values; (*b*) the solid line corresponds to the averaged experimental data and the vertical lines show the SD values. The symbols correspond to the experimental data presented in [37–41]. The squares correspond to the data of [37], the open circles correspond to the data of [38], the up triangles correspond to the data of [39], the open up triangles correspond to the data of [40] and the diamonds correspond to the data of [41].

the absorption bands of oxyhaemoglobin with maximums at 410, 540 and 575 nm are observed [75]. Absorption of water in this spectral range is negligible [76]. In the NIR spectral range, the main chromophores are the water of skin dermis and the lipids of epidermis. In this spectral range the absorption bands of water with maximums at 970 nm [77], 1430 and 1925 nm [78, 79] and lipids with maximums at 1710 and 1780 nm [80] are well seen. At the same time, low-intensity lipid absorption band with the maximum at 930 nm [77] are not observed. Absorption band with the maximum at 1200 nm is the combination of the absorption bands of water (with the maximum at 1197 nm [78, 79]) and lipids (with the maximum at 1212 nm [81]). Increasing the SD in the range of the absorption bands is connected to the differences in the blood and water content in respect of different skin samples. Figure 2(*b*) shows skin absorption coefficient values obtained in this paper (solid line) and those presented by other authors [37–41] (symbols). Comparison of the data obtained in this study and those presented by Simpson *et al* [39] shows an agreement between them. Simpson *et al* [39] reported that in the spectral range 620–1000 nm, skin absorption coefficient is $0.13 \pm 0.12\,\mathrm{cm}^{-1}$. In this spectral range, we obtained $\mu_a \approx 0.37 \pm 0.12\,\mathrm{cm}^{-1}$. Our data are also close to the data of Du *et al* [40] ($\mu_a \approx 0.5 \pm 0.1\,\mathrm{cm}^{-1}$) in the spectral range 900–1100 nm. On the other hand, in this spectral range, Chan *et al* [38] obtained $\mu_a \approx 2.1 \pm 0.5\,\mathrm{cm}^{-1}$. Prahl [37], in the spectral range 620–800 nm obtained, $\mu_a \approx 1.8 \pm 0.4\,\mathrm{cm}^{-1}$. Figure 2(*b*) shows that Chan *et al* [38] (in the spectral range

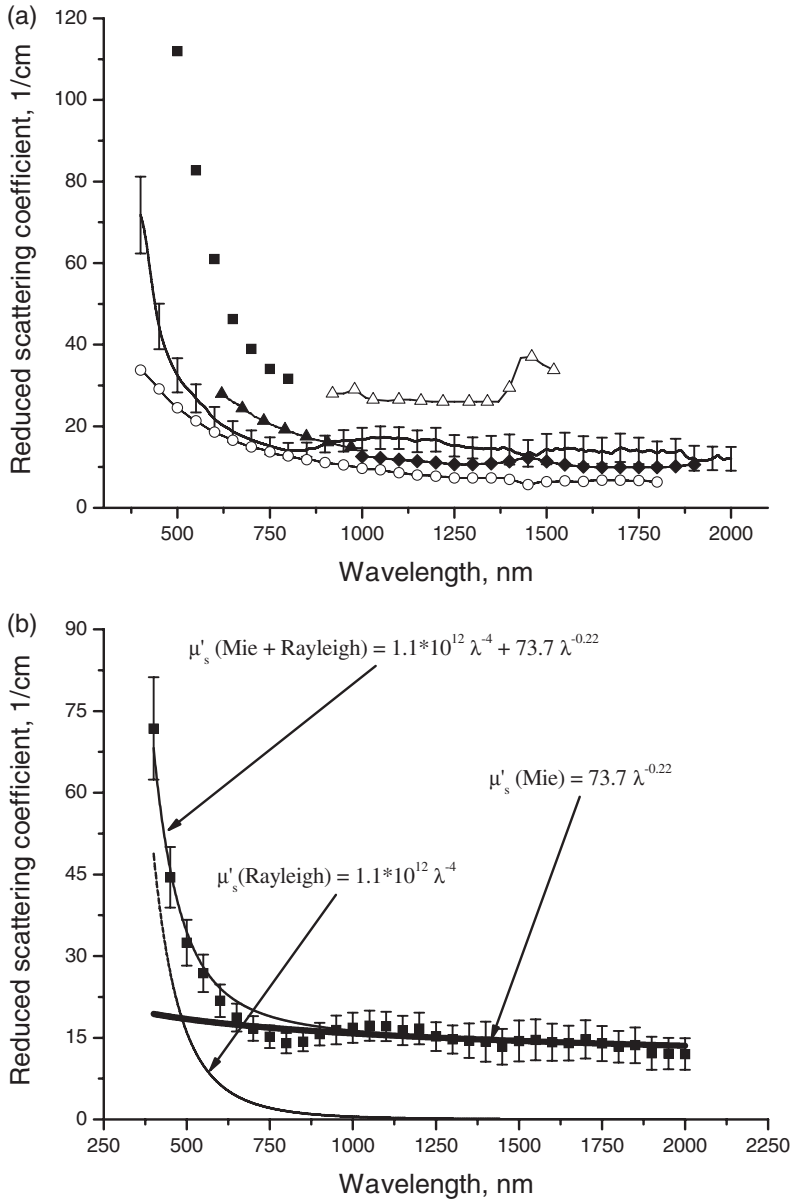

Figure 3. (*a*) The spectral dependence of reduced scattering coefficient μ_s' of human skin *in vitro*. The solid line corresponds to the averaged experimental data and the vertical lines show the SD values. The symbols correspond to the experimental data presented in [37–41]. The squares correspond to the data of [37], the open circles correspond to the data of [38], the up triangles correspond to the data of [39], the open up triangles correspond to the data of [40] and the diamonds correspond to the data of [41]; (*b*) the spectral dependence of reduced scattering coefficient μ_s' of human skin *in vitro* and its approximation by power law. The symbols correspond to the averaged experimental data and the vertical lines show the SD values. The bold and dashed lines show the contribution of the Mie and Rayleigh scattering in the total reduced scattering spectrum, respectively. The solid line shows the combination of the Mie and Rayleigh scattering.

400–600 nm) and Prahl [37] (in the spectral range 450–600 nm) demonstrated the absorption coefficient values, which are larger (up to 2–4 folds) than those presented in this paper. In the spectral range 1200–2000 nm, we obtained absorption coefficient values, which are significantly smaller than those obtained by Chan *et al* [38], Du *et al* [40] and Troy and Thennadil [41], especially in the range of the water absorption band with the maximum at 1450 nm. It is possible that such big discrepancies are related to differences in the water content in respect of different skin samples. At the same time, we have not completely excluded the lateral light loss in the sample that may lead to the overestimation of the absorption coefficient.

Figure 3 presents spectral dependence of the scattering properties (shown as reduced scattering coefficient) of human skin tissue. The dependence was obtained by averaging the scattering spectra measured for the 21 skin samples. The vertical lines show SD values of the reduced scattering coefficients of the skin tissue obtained during the measurements. Figure 3(*a*) shows that the reduced scattering coefficients decreased with an increase in the wavelength, which, in general, corresponds to the common nature of spectral behaviour of the scattering characteristics of tissues [17, 70–72]. However, in the spectral range 400–800 nm the reduced scattering coefficient decreased abruptly with an increase in the wavelength, in contrast

to its spectral behaviour in the spectral range from 800 to 2000 nm, where the reduced scattering coefficient decreased very smoothly as wavelength increased. A comparison of the obtained data (solid line) with the data presented by Chan *et al* [38], Simpson *et al* [39] and Troy and Thennadil [41] (symbols) shows a good agreement between them. At the same time, Prahl [37] and Du *et al* [40] reported values of the reduced scattering coefficient, which are larger than those presented in this paper. The discrepancies are a result of the natural dissipation of tissue properties and the tissue preparation and storage methods.

In the spectral range 600–1500 nm, for many tissues, the reduced scattering coefficient decreases with the wavelength in accordance with a power law $\mu_s'(\lambda) = a\lambda^{-w}$ [69–72]. The wavelength exponent w characterizes the mean size of the tissue scatterers and defines spectral behaviour of the reduced scattering coefficient. Figure 3(*b*) shows approximation of the wavelength dependence of the reduced scattering coefficient by the power law $\mu_s'(\lambda) = 73.7\lambda^{-0.22}$, where λ is wavelength, in nanometres. In the figure it is seen that in the spectral range from 600 to 2000 nm, this power law approximates the experimental data well, in contrast to the data in the spectral range from 400 to 600 nm. Typically, the values of the wavelength exponent obtained for aorta, skin, eye sclera, dura mater, etc are in the range 1–2, which is defined by the major scatterers type [71, 72, 82–86]. Doornbos *et al* [82] and Vargas *et al* [85] reported the wavelength exponent as 1.11 and 1.12, respectively, in the spectral range 500–1200 nm. From the approximation of our data in this spectral range, we obtained $w = 1.1$. Approximating the data of Simpson *et al* [39] in the spectral range 620–1000 nm and Chan *et al* [38] in the spectral range 400–1800 nm, we found w equal to 1.4 and 1.13, respectively. However, for data of Troy and Thennadil [41] in the spectral range 1000–1250 nm, we obtained $w = 0.7$. Thus, it can be seen that the wavelength exponent values obtained vary across different spectral ranges. Assuming that in the visible spectral range (400–700 nm), refractive indices of tissue scatterers and interstitial fluid are 1.45 and 1.36 [17, 71, 72], respectively, the corresponding estimated mean size of the scatterers are in the range 0.2–0.5 μm. The values are equal to skin scatterers size reported by Anderson [87]. At the same time, it should be noted that the values indicate the mean size of the scatterers only. In contrast to this, we obtained a very low value of the wavelength exponent, i.e. $w = 0.22$, for skin in the spectral range 600–2000 nm. This value is very close to the value of the wavelength exponent ($w = 0.23$) in the spectral range 900–1350 nm, following from data of Du *et al* [40] (our estimates). This value is also close to that predicted by Graaff *et al* [88] for the mixture of large spherical particles, i.e. $\mu_s' \sim \lambda^{-0.37}$. One of the possible reasons for these large differences is the complex multi-component structure of skin. As was discussed above, the dominant layer of the skin is the reticular dermis that mainly determines the scattering properties of the whole skin. This layer consists of very thin collagen and elastin fibrils, which are arranged in bundles. Typically, the size of the collagen and elastin fibrils is 60–100 nm and the size of the bundles is in the range 1–8 μm [17, 89]. The presence of large so-called Mie scatterers produces a weak wavelength dependence of the scattering coefficient in the IR spectral range. However, in the spectral range 400–600 nm, the wavelength dependence of the reduced scattering coefficient could not be described by the power law with $w = 0.22$. In this spectral range the reduced scattering coefficient decreased sharply and the effect of the decrease in the reduced scattering coefficient can be explained by the contribution of small, so-called Rayleigh scatterers, i.e. the collagen and elastin fibrils [89,90]. The Rayleigh scattering can be represented as $\mu_s'(\text{Rayleigh}) = b\lambda^{-4}$, where the factor b varies only with the magnitude of the Rayleigh scattering. The measured reduced scattering coefficient spectrum, which is a combination of the Mie and Rayleigh scattering spectra, has been fitted by:

$$\mu_s'(\text{measured}) = \mu_s'(\text{Mie}) + \mu_s'(\text{Rayleigh}) = 73.7\lambda^{-0.22} + b\lambda^{-4} \quad (5)$$

and the factor b has been estimated from the fitting as 1.1×10^{12}. From figure 3(*b*) it is seen that the combination of the wavelength dependences of the Rayleigh and the Mie scattering describes the measured wavelength dependence of the reduced scattering coefficient very well.

The fraction f_{Rayleigh} of the total reduced scattering that is due to Rayleigh scattering by collagen fibrils can be calculated as $f_{\text{Rayleigh}} = (1.1 \times 10^{12}\lambda^{-4})/(1.1 \times 10^{12}\lambda^{-4} + 73.7\lambda^{-0.22})$. The result of the calculations is presented in figure 4. From the figure it is seen that in the visible spectral range the Rayleigh scattering is dominant, but with the increase of the wavelength the contribution of the Rayleigh scattering is decreased sharply and in the NIR the contribution is insignificant. For the wavelength of 633 nm, Saidi *et al* [89] and Graaff *et al* [90] have reported $f_{\text{Rayleigh}} = 0.1$ for skin dermis. For this wavelength we have obtained $f_{\text{Rayleigh}} = 0.2$, but for the whole skin. The larger value indicates that for the whole skin, in the visible spectral range, the contribution of small scatterers of skin epidermis such as melanin dust and structural cell component is significant. It should be noted that the full description of skin scattering implies taking into account light scattering by medium-size scatterers, the so-called Rayleigh–Gans scatterers, such as melanocytes, which are about 300 nm in size. Accounting the contribution of the Rayleigh and

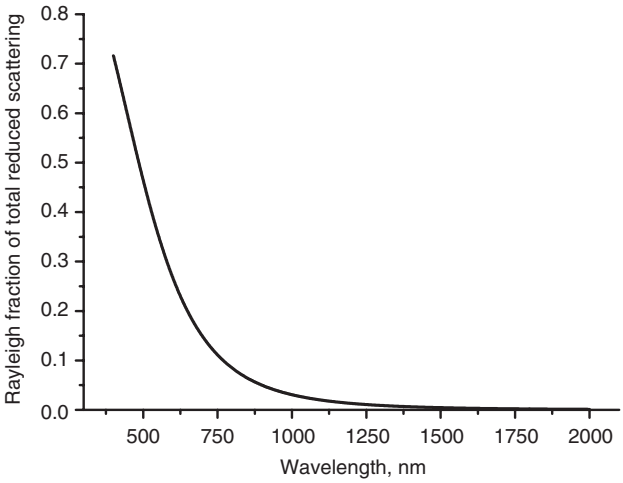

Figure 4. Fraction of total reduced scattering attributed to Rayleigh scattering. The fraction was calculated with data presented in figure 3(*b*) as described in section 4.1.

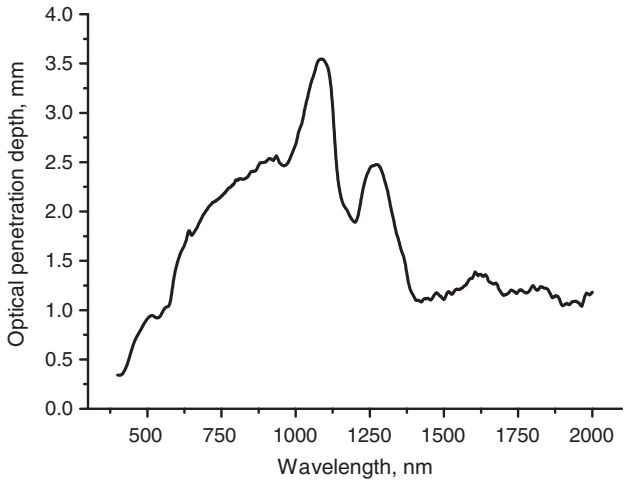

Figure 5. The optical penetration depth δ of light into skin over the wavelength range from 400 to 2000 nm.

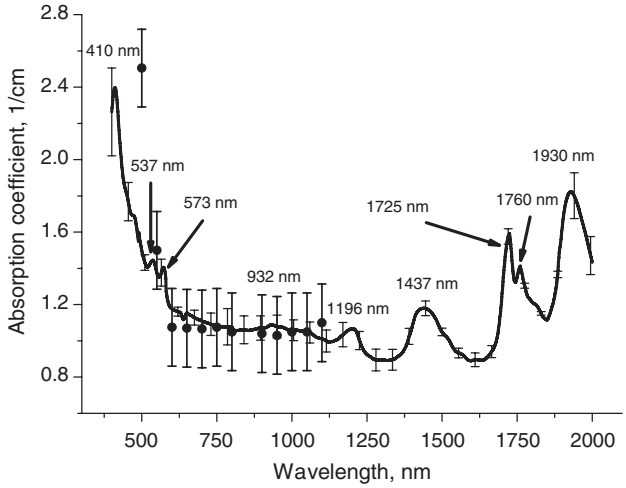

Figure 6. The wavelength dependence of the absorption coefficients μ_a of human subcutaneous adipose tissue calculated using IAD method. The solid line corresponds to the averaged experimental data and the vertical lines show the SD values. The symbols correspond to the experimental data presented in [92].

Rayleigh–Gans scattering, it is necessary to match more precisely the wavelength dependence of skin scattering; the wavelength dependence predicted by a cylindrical Mie-scattering model may also be desirable.

The depth penetration of light into a biological tissue is an important parameter for the correct determination of the irradiation dose in photothermal and photodynamic therapy of various diseases [17]. Estimation of the light penetration depth δ can be performed with the relation [91]

$$\delta = \frac{1}{\sqrt{3\mu_a(\mu_a + \mu_s')}}. \qquad (6)$$

Calculation of the optical penetration depth has been performed with absorption and reduced scattering coefficient values presented in figures 2 and 3 and the result presented in figure 5. The maximal penetration depth 3.5 mm is observed at the wavelength 1090 nm, in figure 5. In a specific spectral range for photodynamic therapy 600–900 nm for the individual wavelengths, such as 600, 633, 660, 700, 750, 800, 850 and 900 nm, the penetration depth is correspondingly equal to 1.5, 1.7, 1.8, 2.0, 2.2, 2.3, 2.4 and 2.5 mm. These data are very close to the data presented in [17].

4.2. Optical properties of the subcutaneous adipose tissue

Six fresh human subcutaneous adipose tissue samples taken from the peritoneum area of patients during the planned surgery were used for the *in vitro* measurements. Figures 6 and 7 present the spectra of the absorption and the reduced scattering coefficients of the subcutaneous adipose tissue calculated by the IAD method on the basis of measured values of the total transmittance and the diffuse reflectance. Figure 6 presents wavelength dependence of the absorption coefficient of human adipose tissue. The vertical lines correspond to the values of SD. In the visible spectral range the absorption bands of oxyhaemoglobin with maxima at 410, 537 and 573 nm are observed [75]. In the NIR spectral range, the main chromophores of the adipose tissue are water and lipids. In this spectral range the absorption bands of water with maximums at 1437 and 1930 nm [78, 79] and lipids

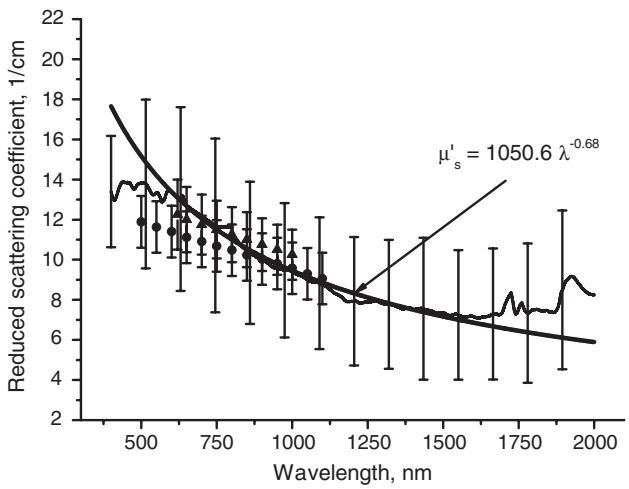

Figure 7. The spectral dependence of the reduced scattering coefficient μ_s' of human subcutaneous adipose tissue calculated using IAD method and its approximation by power law. The vertical lines show the SD values. The symbols correspond to the experimental data presented in [39, 92]. The circles correspond to the data presented in [92] and the up triangles correspond to the data presented in [39].

with maximums at 932 nm [77], 1725 and 1760 nm [80] are well seen. Absorption band with the maximum at 1196 nm is the combination of the absorption bands of water (with the maximum at 1197 nm [78, 79]) and lipids (with the maximum at 1212 nm [81]). Increased SD in the range of the absorption bands is related to differences in the blood and water content in respect of different tissue samples. The symbols in figure 6 correspond to experimental data presented by Peters *et al* [92]. Comparison of data obtained in this study and those presented in [92] shows a good agreement between them. On the other hand, Simpson *et al* [39] show values of absorption coefficients that are much smaller than those measured in this paper. Simpson *et al* [39], using the integrating sphere technique showed that in the spectral range 620–1000 nm, the absorption coefficient of human subcutaneous adipose tissue

is $0.11 \pm 0.03\,\mathrm{cm}^{-1}$. In contrast, in this spectral range, we obtained a mean value of the absorption coefficient that was ten times bigger at $1.1 \pm 0.03\,\mathrm{cm}^{-1}$. Such a big discrepancy could be related to differences in used tissue sample storage and preparation methods. Simpson *et al* [39] reported that in their study the tissue samples were refrigerated for five days storage and allowed to return to room temperature before being dissected for optical measurements. At the same time, in our measurements we have not completely excluded the lateral light loss in the sample that may lead to overestimation of the absorption coefficient.

Figure 7 presents spectral dependence of the reduced scattering coefficient of human adipose tissue. The dependence was obtained by averaging the spectra of the reduced scattering coefficients measured for the six tissue samples. The vertical lines show SD values. It is clearly seen that in the spectral range 400–1500 nm, the reduced scattering coefficients decreased smoothly with an increase in the wavelength, which, in general, corresponds to the common nature of spectral behaviour of the scattering characteristics of tissues [17, 70–72]. However, in the spectral range 1500–2000 nm, the reduced scattering coefficient increases smoothly with an increase in the wavelength with peaks corresponding to the absorption bands. A comparison of the obtained data with the data presented in [39, 92] shows a good agreement between them.

Figure 7 shows approximation of the wavelength dependence of the reduced scattering coefficient by the power law $\mu_s'(\lambda) = 1050.6\lambda^{-0.68}$, where λ is wavelength,in nanometres. In the figure it is seen, that in the spectral range 600–1500 nm this power law approximates the experimental data well, in contrast to the data in the spectral ranges 400–600 nm and 1500–2000 nm. In this study we obtained, for adipose tissue, a low value of the wavelength exponent: $w = 0.68$. A possible reason for this is the specificity of adipose tissue structure, which consists mostly of fat cells. Each fat cell contains a number of smooth droplets of lipids, the size of which is apparently larger than that of typical tissue scatterers (the mitochondria of cells, and the collagen and elastin fibrils of fibrous tissues). For such large and rather homogeneous scatterers a weak wavelength dependence of light scattering coefficients might be expected. Another reason is the possible influence of dispersion of lipids and water bands, which should decrease the inclination of the wavelength dependence in the spectral range of around 1000–1500 nm.

For estimation of the mean size of scatterers of adipose tissue, the spectroturbidimetric method [69], briefly described in the section 3, has been used. In the wavelength range 456–1064 nm, the refractive indices of the tissue scatterers and interstitial fluid are 1.455 and 1.36, respectively, [17, 44]. Using the refractive index values and the spectroturbidimetric method, the mean size of adipose tissue scatterers (the lipid droplets) has been estimated at 0.8 μm. The value can be used for the estimation of the number of scatterers in the single adipocyte. Since the mean diameter of a single adipocyte is varied from 50 [50] to 120 μm [51], the number is in the range 2×10^5–3×10^6 scatterers per cell. It should be noted that the number and the size of the droplets are changed at obesity and cellulite.

The effect of the deviation of wavelength dependence of the reduced scattering coefficient from the power law dependence, i.e. the increase of the reduced scattering coefficients in the spectral range 1500–2000 nm, can be explained by the increase of the imaginary part of complex refractive index of the tissue scatterers in the range of absorption bands. The increase of the imaginary part of the refractive index produces a significant decrease of the anisotropy factor g, which together with the scattering coefficient μ_s of a tissue forms the tissue reduced scattering coefficient $\mu_s' = \mu_s(1-g)$. In [40, 91] it was experimentally shown that in the range of water absorption bands, with the maximum at 1450 and 1930 nm, a significant decrease in the anisotropy factor is observed, which produces an increase in the reduced scattering coefficient and appearance of bands in its spectrum. Note that the degree of decrease in the anisotropy factor in the range of absorption bands is proportional to the intensity of the absorption bands. The tissue scattering coefficient in the range of the absorption bands is decreased only slightly [40, 91]. This behaviour is explained by anomalous light dispersion, since within an absorption band the real part of the refractive index corresponding to the short-wavelength wing of the absorption band goes down, and at the long-wavelength wing it goes up. Owing to this fact the significant decrease of the anisotropy factor and the scattering coefficient within the absorption band should be observed. This was confirmed by Faber *et al* [93] who calculated the wavelength dependences of the scattering coefficient and the anisotropy factor of blood, taking into account the spectral dependence of the real and imaginary parts of the complex refractive index of haemoglobin. The data presented in figure 7 are well explained using the concept of anomalous light dispersion discussed earlier. In figure 6 one can see, that in the spectral range 600–1400 nm, the absorption of adipose tissue is small. Hence, the scattering properties of the tissue are defined only by the real part of complex refractive index and the reduced scattering coefficient decreases rather monotonically with the wavelength. In the spectral range 1400–2000 nm, the strong absorption bands of water and lipids are observed (see figure 6). The presence of the strong absorption bands leads to the fact that the scattering properties are formed under the influence of not only the real but also the imaginary part of a complex refractive index of the scattering centres, which produces an increase in the reduced scattering coefficient in the given spectral region with strong enough peaks in the range of the absorption bands. The scattering properties of the tissue in this wavelength range are defined by the real part of refractive index of water and lipids, which have a complex behaviour owing to the anomalous light dispersion and background scattering which is defined by the light scattering on the lipid droplets and the tissue matrix which contained the blood capillaries, nerves and reticular fibrils (about 50% of the adipose tissue is the stroma, which contained the collagen and elastin fibrils [50, 51]). The background scattering decreases with the wavelength in accordance with the power law.

In the spectral range 350–600 nm, blood erythrocytes have a contribution in the fat scattering spectrum, owing to their absorption and scattering properties [94]. The reduced scattering coefficient of whole blood decreases significantly within the absorption bands [95]. Thus the reduced scattering coefficient of adipose tissue decreases as well.

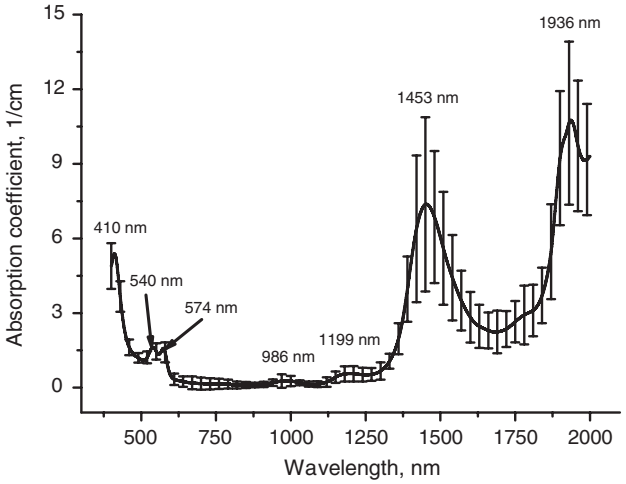

Figure 8. The wavelength dependence of the absorption coefficients μ_a of human mucous tissue calculated using IAD method. The solid line corresponds to the averaged experimental data and the vertical lines show the SD values.

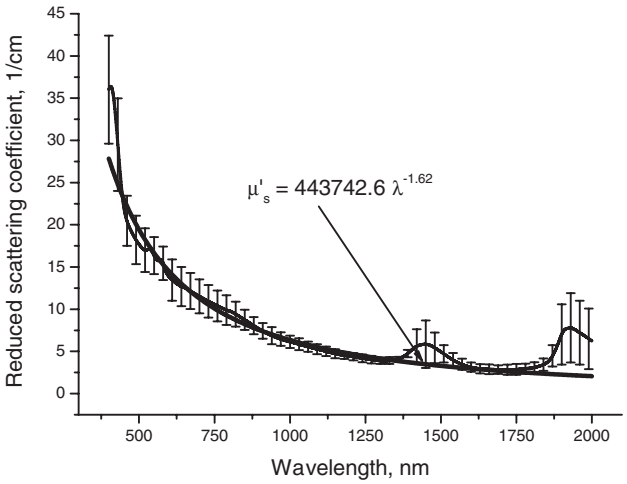

Figure 9. The spectral dependence of the reduced scattering coefficient μ_s' of human mucous tissue calculated using IAD method and its approximation by power law. The vertical lines show the SD values.

4.3. Optical properties of maxillary sinuses mucous membrane

Optical properties of the mucous membrane of the maxillary sinuses were measured from ten samples, which were obtained from ten patients with chronic maxillary sinusitis during the planned surgery. Figures 8 and 9 show the spectra of the absorption and reduced scattering coefficients, calculated by the IAD method from the experimentally measured diffuse reflectance and total transmittance. Figure 8 shows the absorption spectrum of the mucous tissue in the spectral range 400–2000 nm. The vertical lines indicate the SD values. In the spectrum, absorption bands of blood oxyhaemoglobin (415, 540 and 575 nm [75]) and water (1450 and 1930 nm [78, 79]) are clearly seen. The absorption bands of water located at 976 and 1197 nm [78, 79] are considerably less observed. Recently, optical properties of mucous tissue have been presented by Müller and Roggan [44] and Shah *et al* [96], for the wavelength 1064 nm. For the wavelength, the absorption coefficient of the mucous layer of the bladder, colon, oesophagus, stomach [44] and tonsillar [96] are 0.7 cm^{-1}, 2.7 cm^{-1}, 1.1 cm^{-1}, 2.8 cm^{-1} [44] and 0.39 cm^{-1} [96], respectively. For the wavelength, we obtained $\mu_a = 0.14 \pm 0.1\,cm^{-1}$.

Figure 9 presents the spectral dependence of the reduced scattering coefficient of the mucous tissue. This dependence was obtained by averaging the spectra of the reduced scattering coefficient of the ten samples of the mucous tissue. It is clearly seen that, with increase in wavelength, the reduced scattering coefficient decreases smoothly, which corresponds to the general spectral behaviour of the scattering characteristics of biological tissues [17, 70–72]. However, in the range of the strong absorption bands (415, 1450 and 1930 nm), the shape of the scattering spectrum deviates from a monotonic dependence. At the same time, in the range of the water absorption bands with maximums at 976 and 1197 nm the effect is not observed. For the wavelength 1064 nm, Müller and Roggan [44] and Shah *et al* [96] reported that the reduced scattering coefficients of the mucous layer of the bladder, colon, oesophagus, stomach [44] and tonsillar [96] are 1.1 cm^{-1}, 3.5 cm^{-1}, 11.6 cm^{-1}, 65.9 cm^{-1} [44] and 5.2 cm^{-1} [96], respectively. For this wavelength we obtained $\mu_s' = 5.51 \pm 0.6\,cm^{-1}$.

Figure 9 shows the approximation of the wavelength dependence of the reduced scattering coefficient by the power law $\mu_s'(\lambda) = 443742.6\lambda^{-1.62}$, where λ is wavelength, in nanometres. In the figure it is seen that in the spectral range 600–1300 nm, this power law approximates the experimental data well, in contrast to the data in the spectral ranges 400–600 nm and 1300–2000 nm. The value of the wavelength exponent ($w = 1.62$) obtained in this study, is a typical for many tissues. Assuming that the visible spectral range refractive indices of the tissue scatterers and the interstitial fluid are 1.45 and 1.36 [17, 71, 72], respectively, the corresponding estimated mean diameter of the scatterers is 0.3 μm. Taking into account this value and the structure of the tissue, we can assume that the main scatterers of the tissue are mitochondria and leukocytes. At the same time, collagen and elastin fibrils of the proper layer of the mucous membrane also contribute in the scattering properties of the tissue, especially in the short-wavelength range of the spectrum.

The deviation of the spectrum of the reduced scattering coefficient from a monotonic dependence can be explained by the increase of the real part of the complex refractive index of the tissue scatterers, owing to the anomalous light dispersion. In the range of strong absorption bands, the effect produces a significant decrease in the anisotropy factor, which leads to an increase in the reduced scattering coefficient.

Calculation of the optical penetration depth has been performed with the absorption and the reduced scattering coefficient values presented in figures 8 and 9, respectively, and the result is presented in figure 10. From figure 10 it is seen that depending on the wavelength, the penetration depth varies considerably. The depth is maximal in the spectral ranges 800–900 nm and 1000–1100 nm, where the optical radiation penetrates to depths of up to 6–6.5 mm, which significantly exceeds the thickness of the mucous membrane, both in the normal and in the pathological state. In the range

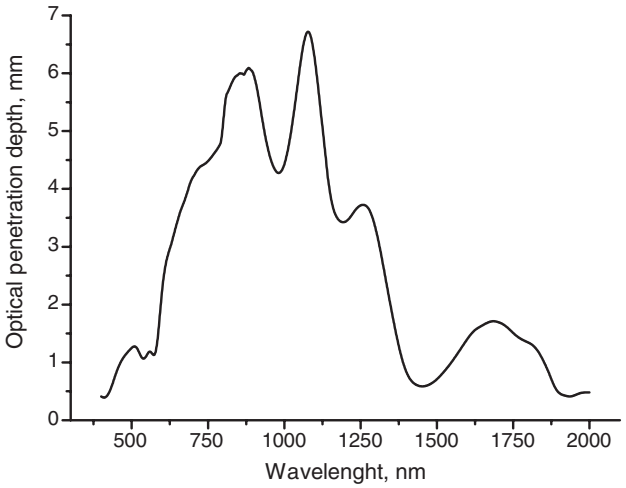

Figure 10. The optical penetration depth δ of light into human mucous tissue over the wavelength range from 400 to 2000 nm.

of wavelengths of a He–Ne (633 nm) and diode (660 nm) lasers, which are most frequently used in photodynamic therapy [17], the penetration depth amounts to 3–3.5 mm, which also exceeds the thickness of the mucous membrane.

5. Conclusion

The reduced scattering and the absorption coefficients of the human skin, subcutaneous and mucous tissues *in vitro* have been determined over the wavelength range 400–2000 nm, using the integrating sphere technique and the IAD method. In this spectral range, the absorption bands of oxyhaemoglobin, water and lipids with maxima at 410(415), 537(540), 573(575), 932, 970(976), 1196(1200), 1430(1437, 1450), 1710(1725), 1760(1780) and 1925(1930) nm are observed. For skin in the spectral range from 400 to 2000 nm, wavelength dependence of the reduced scattering coefficient can be described as $\mu_s'(\lambda) = 73.7\lambda^{-0.22} + 1.1 \times 10^{12}\lambda^{-4}$. The first term corresponds to Mie scattering and the second to Rayleigh scattering. We also demonstrated that in the visible spectral range the Rayleigh scattering is dominant. The penetration depth of light into skin has been estimated.

For human subcutaneous adipose tissue it was shown that in the spectral range from 400 to 1500 nm the reduced scattering coefficient decreases smoothly with the wavelength, but in the spectral range 1500–2000 nm it increases with oscillations (peaks corresponding to the absorption bands). The presence of the strong absorption bands leads to the scattering properties depending not only on the real but also on the imaginary part of a complex refractive index of the tissue scatterers owing to anomalous light dispersion. In the spectral range 600–1500 nm the power law $\mu_s'(\lambda) = 1050.6\lambda^{-0.68}$ well approximates the experimental data. The effect of deviation of wavelength dependence of the reduced scattering coefficient from power law dependence in the spectral range 1500–2000 nm can be explained by the strong influence of the imaginary part of the complex refractive index of the scatterers. In the spectral range 400–600 nm, the deviation has been explained by the influence of blood erythrocytes, which have contributed to the scattering and absorption spectra of the adipose tissue.

For human mucous tissue in the spectral range 400–2000 nm, the reduced scattering coefficient decreases with the wavelength, but in the range of the strong absorption bands with maximums at 415, 1450 and 1930 nm the reduced scattering coefficient increases as a result of the anomalous light dispersion. In the spectral range 600–1300 nm, the power law $\mu_s'(\lambda) = 443742.6\lambda^{-1.62}$, well approximates the experimental data. For this tissue the optical penetration depth has also been estimated.

The results presented can be used for the development of optical technologies and can be useful in photodynamic and photothermal therapy.

Acknowledgments

The research described in this publication has been made possible, in part, by grant REC-006/SA-006-00 'Nonlinear Dynamics and Biophysics' of the US Civilian Research and Development Foundation for the Independent States of the Former Soviet Union (CRDF) and the Russian Ministry of Science and Education; the Russian Federation President's grant N 25.2003.2 'Supporting of Scientific Schools' and grant 'Leading Research-Educational Teams' N 2.11.03 of the Russian Ministry of Science and Education. The authors thank Dr S V Eremina (Department of English and Intercultural Communication of Saratov State University) for the help in translating the manuscript into English.

References

[1] Hamaoka T *et al* 2000 Quantification of ischemic muscle deoxygenation by near infrared time-resolved spectroscopy *J. Biomed. Opt.* **5** 102–5

[2] Liu H, Song Y, Worden K L, Jiang X, Constantinescu A and Mason R P 2000 Noninvasive investigation of blood oxygenation dynamics of tumors by near-infrared spectroscopy *Appl. Opt.* **39** 5231–43

[3] Kolinko V G, de Mul F F M, Greve J and Priezzhev A V 1998 Feasibility of picosecond laser-Doppler flowmetry provides basis for time-resolved Doppler tomography of biological tissues *J. Biomed. Opt.* **3** 187–90

[4] Zourabian A, Siegel A, Chance B, Ramanujan N, Rode M and Boas D A 2000 Trans-abdominal monitoring of fetal arterial blood oxygenation using pulse oximetry *J. Biomed. Opt.* **5** 391–405

[5] Betz C S, Mehlmann M, Rick K, Stepp H, Grevers G, Baumgartner R and Leunig A 1999 Autofluorescence imaging and spectroscopy of normal and malignant mucosa in patients with head and neck cancer *Lasers Surg. Med.* **25** 323–34

[6] Andersson-Engels S *et al* 2000 Preliminary evaluation of two fluorescence imaging methods for the detection and the delineation of basal cell carcinomas of the skin *Lasers Surg. Med.* **26** 76–82

[7] Bigio I J, Bown S G, Briggs G, Kelley C, Lakhani S, Pickard D, Ripley P M, Rose I G and Saunders C 2000 Diagnosis of breast cancer using elastic-scattering spectroscopy: preliminary clinical results *J. Biomed. Opt.* **5** 221–8

[8] Benavides J M, Chang S, Park S Y, Richards-Kortum R, Mackinnon N, MacAulay C, Milbourne A, Malpica A and Follen M 2003 Multispectral digital colposcopy for *in vivo* detection of cervical cancer *Opt. Express* **11** 1223–36

[9] Arnoldussen M E, Cohen D, Bearman G H and Grundfest W S 2000 Consequences of scattering for spectral imaging of turbid biological tissue *J. Biomed. Opt.* **5** 300–6

[10] Benaron D A *et al* 2000 Noninvasive functional imaging of human brain using light *J. Cerebr. Blood F. Met.* **20** 469–77
[11] Demos S G, Gandour-Edwards R, Ramsamooj R and White R 2004 Spectroscopic detection of bladder cancer using near-infrared imaging techniques *J. Biomed. Opt.* **9** 767–71
[12] Buscher B A, McMeekin T O and Goodwin D 2000 Treatment of leg telangiectasia by using a long-pulse dye laser at 595 nm with and without dynamic cooling device *Lasers Surg. Med.* **27** 171–5
[13] Abela G S, Hage-Korban E E, Tomaru T, Barbeau G R, Abela O G and Friedl S E 2001 Vascular procedures that thermo-coagulate collagen reduce local platelet deposition and thrombus formation: laser and laser-thermal versus balloon angioplasty *Lasers Surg. Med.* **29** 455–63
[14] Ross E V, Domankevitz Y and Anderson R R 1997 Effects of heterogeneous absorption of laser radiation in biotissue ablation: characterization of ablation of fat with a pulsed CO_2 laser *Lasers Surg. Med.* **21** 59–64
[15] Dietlein T S, Jacobi P C and Krieglstein G K 1998 Erbium : YAG laser trabecular ablation (LTA) in the surgical treatment of glaucoma *Lasers Surg. Med.* **23** 104–10
[16] Shah R K, Nemati B, Wang L V and Shapshay S M 2001 Optical-thermal simulation of tonsillar tissue irradiation *Lasers Surg. Med.* **28** 313–19
[17] Tuchin V V 2000 *Tissue Optics: Light Scattering Methods and Instruments for Medical Diagnosis* vol TT38 (Washington: SPIE Press)
[18] Langmack K, Mehta R, Twyman P and Norris P 2001 Total photodynamic therapy at low fluence rates—theory and practice *J. Photochem. Photobiol.* B **60** 37–43
[19] de Rosa F S and Bentley M V L B 2000 Photodynamic therapy of skin cancers: sensitizers, clinical studies and future directives *Pharmaceut. Res.* **17** 1447–55
[20] Brancaleon L and Moseley H 2002 Laser and non-laser light sources for photodynamic therapy *Lasers Med. Sci.* **17** 173–86
[21] Fehr M K, Hornung R, Degen A, Schwarz V A, Fink D, Haller U and Wyss P 2002 Photodynamic therapy of vulgar and vaginal condyloma and intraepithelial neoplasia using topically applied 5-aminolevulinic acid *Lasers Surg. Med.* **30** 273–79
[22] Ibbotson S H 2002 Topical 5-aminolaevulinic acid photodynamic therapy for the treatment of skin conditions other than non-melanoma skin cancer *Br. J. Dermatol.* **146** 178–88
[23] Tuchin V V, Genina E A, Bashkatov A N, Simonenko G V, Odoevskaya O D and Altshuler G B 2003 A pilot study of ICG laser therapy of *acne vulgaris*: photodynamic and photothermolysis treatment *Lasers Surg. Med.* **33** 296–310
[24] Genina E A, Bashkatov A N, Simonenko G V, Odoevskaya O D, Tuchin V V and Altshuler G B 2004 Low-intensity indocyanine-green laser phototherapy of *acne vulgaris*: pilot study *J. Biomed. Opt.* **9** 828–34
[25] Kormeili T, Yamauchi P S and Lowe N J 2004 Topical photodynamic therapy in clinical dermatology *Br. J. Dermatol.* **150** 1061–69
[26] Bays R, Wagnieres G, Robert D, Braichotte D, Savary J-F, Monnier P and van den Bergh H 1997 Light dosimetry for photodynamic therapy in the esophagus *Lasers Surg. Med.* **20** 290–303
[27] Brunetaud J M, Maunoury V and Cochelard D 1997 Lasers in digestive endoscopy *J. Biomed. Opt.* **2** 42–52
[28] Calzavara-Pinton P G, Szeimies R-M, Ortel B and Zane C 1996 Photodynamic therapy with systemic administration of photosensitizers in dermatology *J. Photochem. Photobiol.* B **36** 225–31
[29] Corti L, Mazzarotto R, Belfontali S, De Luca C, Baiocchi C, Boso C and Calzavara F 1996 Photodynamic therapy in gynaecological neoplastic diseases *J. Photochem. Photobiol.* B **36** 193–7
[30] Koderhold G, Jindra R, Koren H, Alth G and Schenk G 1996 Experiences of photodynamic therapy in dermatology *J. Photochem. Photobiol.* B **36** 221–3
[31] Koren H and Alth G 1996 Photodynamic therapy in gynaecologic cancer *J. Photochem. Photobiol.* B **36** 189–91
[32] Kubler A C, Haase T, Staff C, Kahle B, Rheinwald M and Muhling J 1999 Photodynamic therapy of primary nonmelanomatous skin tumours of the head and neck *Lasers Surg. Med.* **25** 60–8
[33] Maier A, Anegg U, Fell B, Rehak P, Ratzenhofer B, Tomaselli F, Sankin O, Pinter H, Smolle-Juttner F M and Friehs G B 2000 Hyperbaric oxygen and photodynamic therapy in the treatment of advanced carcinoma of the cardia and the esophagus *Lasers Surg. Med.* **26** 308–15
[34] Szeimies R-M, Calzavara-Pinton P, Karrer S, Ortel B and Landthaler M 1996 Topical photodynamic therapy in dermatology *J. Photochem. Photobiol.* B **36** 213–9
[35] Zeina B, Greenman J, Purcell W M and Das B 2001 Killing of cutaneous microbial species by photodynamic therapy *Br. J. Dermatology* **144** 274–8
[36] Zeitouni N C, Shieh S and Oseroff A R 2001 Laser and photodynamic therapy in the management of cutaneous malignancies *Clin. Dermatol.* **19** 328–39
[37] Prahl S A 1988 Light transport in tissue *PhD Thesis* University of Texas at Austin
[38] Chan E K, Sorg B, Protsenko D, O'Neil M, Motamedi M and Welch A J 1996 Effects of compression on soft tissue optical properties *IEEE J. Quantum Electron.* **2** 943–50
[39] Simpson C R, Kohl M, Essenpreis M and Cope M 1998 Near-infrared optical properties of *ex vivo* human skin and subcutaneous tissues measured using the Monte Carlo inversion technique *Phys. Med. Biol.* **43** 2465–78
[40] Du Y, Hu X H, Cariveau M, Kalmus G W and Lu J Q 2001 Optical properties of porcine skin dermis between 900 nm and 1500 nm *Phys. Med. Biol.* **46** 167–81
[41] Troy T L and Thennadil S N 2001 Optical properties of human skin in the near infrared wavelength range of 1000 to 2200 nm *J. Biomed. Opt.* **6** 167–76
[42] Nasedkin A N *et al* 2002 The experience of application of photodynamic therapy for treatment of acute and chronic purulent antritis *Russ. Rhinol.* **2** 116 (in Russian)
[43] Piskunov G Z and Piskunov S Z 2002 *Clinical Rhinology* (Moscow: Miklon) (in Russian)
[44] Müller G and Roggan A (ed) 1995 *Laser-Induced Interstitial Thermotherapy* (Washington: SPIE Press)
[45] Stenn K S 1988 The skin *Cell and Tissue Biology* ed L Weiss (Baltimore: Urban & Shwarzenberg) pp 541–72
[46] Odland G F 1991 Structure of the skin *Physiology, Biochemestry, and Molecular Biology of the Skin* vol 1, ed L A Goldsmith (Oxford: Oxford University Press) pp 3–62
[47] Ryan T J 1991 Cutaneous Circulation *Physiology, Biochemestry, and Molecular Biology of the Skin* vol 2, ed L A Goldsmith (Oxford: Oxford University Press) pp 1019–84
[48] Young A R 1997 Chromophores in human skin *Phys. Med. Biol.* **42** 789–802
[49] Chedekel M R 1995 Photophysics and photochemistry of melanin *Melanin: Its Role in Human Photoprotection* ed L Zeise *et al* (Overland Park: Valdenmar) pp 11–22
[50] Taton' Y 1981 *Obesity, Pathphysiology, Diagnostics, Therapy* (Warsaw: Medical Press)
[51] Shurigin D Ya, Vyazitskiy P O and Sidorov K A 1975 *Obesity* (Leningrad: Medicine) (in Russian)
[52] Gurr M I, Jung R T, Robinson M P and James W P T 1982 Adipose tissue cellularity in man: the relationship between fat cell size and number, the mass and distribution of body fat and the history of weight gain and loss *Int. J. Obesity* **6** 419–36
[53] Piskunov G Z and Piskunov S Z 1991 *Diagnostics and Medical Treatment of Inflammatory Processes of the*

Mucous Membrane of Nose and Maxillary Sinuses (Voronezh: Voronezh State University Press) (in Russian)
[54] Zavaliy M A, Balabantsev A G, Zagorul'ko A K and Filonenko T G 2002 State of ciliary epithelium of patients with the chronic purulent sinusitis *Russ. Rhinol.* **2** 19–22 (in Russian)
[55] Prahl S A, van Gemert M J C and Welch A J 1993 Determining the optical properties of turbid media by using the adding–doubling method *Appl. Opt.* **32** 559–68
[56] Nemati B, Rylander H G III and Welch A J 1996 Optical properties of conjunctiva, sclera, and the ciliary body and their consequences for transscleral cyclophotocoagulation *Appl. Opt.* **35** 3321–7
[57] Beek J F, Blokland P, Posthumus P, Aalders M, Pickering J W, Sterenborg H J C M and van Gemert M J C 1997 *In vitro* double-integrating-sphere optical properties of tissues between 630 and 1064 nm *Phys. Med. Biol.* **42** 2255–61
[58] Sardar D K, Mayo M L and Glickman R D 2001 Optical characterization of melanin *J. Biomed. Opt.* **6** 404–11
[59] Bashkatov A N, Genina E A, Kochubey V I and Tuchin V V 2000 Estimation of wavelength dependence of refractive index of collagen fibers of scleral tissue *Proc. SPIE* **4162** 265–8
[60] Bashkatov A N, Genina E A, Korovina I V, Kochubey V I, Sinichkin Yu P and Tuchin V V 2000 *In vivo* and *in vitro* study of control of rat skin optical properties by acting of osmotical liquid *Proc. SPIE* **4224** 300–11
[61] Farrell T J, Patterson M S and Wilson B C 1992 A diffusion theory model of spatially resolved, steady-state diffuse reflectance for the noninvasive determination of tissue optical properties *in vivo Med. Phys.* **19** 879–88
[62] Dam J S, Andersen P E, Dalgaard T and Fabricius P E 1998 Determination of tissue optical properties from diffuse reflectance profiles by multivariate calibration *Appl. Opt.* **37** 772–8
[63] Bevilacqua F, Piguet D, Marquet P, Gross J D, Tromberg B J and Depeursinge C 1999 *In vivo* local determination of tissue optical properties: applications to human brain *Appl. Opt.* **38** 4939–50
[64] Ebert D W, Roberts C, Farrar S K, Johnston W M, Litsky A S and Bertone A L 1998 Articular cartilage optical properties in the spectral range 300–850 nm *J. Biomed. Opt.* **3** 326–33
[65] Farrar S K, Roberts C, Johnston W M and Weber P A 1999 Optical properties of human trabecular meshwork in the visible and near-infrared region *Lasers Surg. Med.* **25** 348–62
[66] Vargas W E 2002 Inversion methods from Kubelka–Munk analysis *J. Opt. A: Pure Appl. Opt.* **4** 452–6
[67] Yaroslavsky I V, Yaroslavsky A N, Goldbach T and Schwarzmaier H-J 1996 Inverse hybrid technique for determining the optical properties of turbid media from integrating-sphere measurements *Appl. Opt.* **35** 6797–809
[68] Pickering J W, Prahl S A, van Wieringen N, Beek J F, Sterenborg H J C M and van Gemert M J C 1993 Double-integrating-sphere system for measuring the optical properties of tissue *Appl. Opt.* **32** 399–410
[69] Shchyogolev S Yu 1999 Inverse problems of spectroturbidimetry of biological disperse systems: an overview *J. Biomed. Opt.* **4** 490–503
[70] Mourant J R, Fuselier T, Boyer J, Johnson T M and Bigio I J 1997 Predictions and measurements of scattering and absorption over broad wavelength ranges in tissue phantoms *Appl. Opt.* **36** 949–57
[71] Schmitt J M and Kumar G 1998 Optical scattering properties of soft tissue: a discrete particle model *Appl. Opt.* **37** 2788–97
[72] Wang R K 2000 Modelling optical properties of soft tissue by fractal distribution of scatterers *J. Mod. Opt.* **47** 103–20
[73] Bohren C F and Huffman D R 1983 *Absorption and Scattering of Light by Small Particles* (New York: Wiley)
[74] Press W H, Tuekolsky S A, Vettering W T and Flannery B P 1992 *Numerical Recipes in C: The Art of Scientific Computing* (Cambridge: Cambridge University Press)
[75] Prahl S A 1999 Optical absorption of hemoglobin http://www.omlc.ogi.edu/spectra/
[76] Smith R C and Baker K S 1981 Optical properties of the clearest natural waters (200 800 nm) *Appl. Opt.* **20** 177–84
[77] McBride T O, Pogue B W, Poplack S, Soho S, Wells W A, Jiang S, Osterberg U L and Paulsen K D 2002 Multispectral near-infrared tomography: a case study in compensating for water and lipid content in hemoglobin imaging of the breast *J. Biomed. Opt.* **7** 72–9
[78] Kou L, Labrie D and Chylek P 1993 Refractive indices of water and ice in the 0.65 -2.5 μm spectral range *Appl. Opt.* **32** 3531–40
[79] Palmer K F and Williams D 1974 Optical properties of water in the near infrared *J. Opt. Soc. Am.* **64** 1107–10
[80] Martin K A 1993 Direct measurement of moisture in skin by NIR spectroscopy *J. Soc. Cosmet. Chem.* **44** 249–61
[81] Lauridsen R K, Everland H, Nielsen L F, Engelsen S B and Norgaard L 2003 Exploratory multivariate spectroscopic study on human skin *Skin Res. Technol.* **9** 137–46
[82] Doornbos R M P, Lang R, Aalders M C, Cross F W and Sterenborg H J C M 1999 The determination of *in vivo* human tissue optical properties and absolute chromophore concentrations using spatially resolved steady-state diffuse reflectance spectroscopy *Phys. Med. Biol.* **44** 967–81
[83] Cilesiz I F and Welch A J 1993 Light dosimetry: effects of dehydration and thermal damage on the optical properties of the human aorta *Appl. Opt.* **32** 477–87
[84] Bashkatov A N 2002 Control of tissue optical properties by means of osmotically active immersion liquids *PhD Thesis* Saratov State University, Saratov, Russia
[85] Vargas G, Chan E K, Barton J K, Rylander H G III and Welch A J 1999 Use of an agent to reduce scattering in skin *Lasers Surg. Med.* **24** 133–41
[86] Ghosh N, Mohanty S K, Majumder S K and Gupta P K 2001 Measurement of optical transport properties of normal and malignant human breast tissue *Appl. Opt.* **40** 176–84
[87] Anderson R R 1993 Optics of the skin *Clinical Photomedicine* ed H W Lim and N A Soter (New York: Marcel Dekker) pp 19–35
[88] Graaff R, Aarnoudse J G, Zijp J R, Sloot P M A, de Mul F F M, Greve J and Koelink M H 1992 Reduced light-scattering properties for mixtures of spherical particles: a simple approximation derived from Mie calculations *Appl. Opt.* **31** 1370–6
[89] Saidi I S, Jacques S L and Tittel F K 1995 Mie and Rayleigh modeling of visible-light scattering in neonatal skin *Appl. Opt.* **34** 7410–8
[90] Graaff R, Dassel A C M, Koelink M H, de Mul F F M, Aarnoudse J G and Zijlstra W G 1993 Optical properties of human dermis *in vitro* and *in vivo Appl. Opt.* **32** 435–47
[91] Ritz J-P, Roggan A, Isbert C, Muller G, Buhr H and Germer C-T 2001 Optical properties of native and coagulated porcine liver tissue between 400 and 2400 nm *Lasers Surg. Med.* **29** 205–12
[92] Peters V G, Wyman D R, Patterson M S and Frank G L 1990 Optical properties of normal and diseased human breast tissues in the visible and near infrared *Phys. Med. Biol.* **35** 1317–34
[93] Faber D J, Aalders M C G, Mik E G, Hooper B A, van Gemert M J C and van Leeuwen T G 2004 Oxygen saturation-dependent absorption and scattering of blood *Phys. Rev. Lett.* **93** 028102-1–028102-4
[94] Roggan A, Friebel M, Dorschel K, Hahn A and Muller G 1999 Optical properties of circulating human blood in the wavelength range 400–2500 nm *J. Biomed. Opt.* **4** 36–46
[95] Bashkatov A N, Zhestkov D M, Genina E A and Tuchin V V 2005 Immersion clearing of human blood in visible and near-infrared spectral ranges *Opt. Spectrosc.* **98** 638–46
[96] Shah R K, Nemati B, Wang L V and Shapshay S M 2001 Optical-thermal simulation of tonsillar tissue irradiation *Lasers Surg. Med.* **28** 313–9